Fluorescence Photoconversion Kinetics in Novel Green Fluorescent Protein pH Sensors (pHluorins)

Samuel T. Hess,[‡,⊥,#] Ahmed A. Heikal,[†,§,#] and Watt W. Webb*[,†]

Department of Physics and School of Applied & Engineering Physics, Cornell University, Ithaca, New York 14853

Received: July 28, 2003; In Final Form: January 2, 2004

Genetically encoded pH-sensitive green fluorescent proteins (GFPs) offer significant control over localization, spectral properties, and environmental sensitivity for cell biology and neuroscience applications. Quantitative analysis of biological applications and full exploitation of novel GFP properties rely on a fundamental understanding of their molecular photophysics. In this contribution, the ground- and excited-state fluorescence properties of Ecliptic and Ratiometric pHluorins, two pH-sensitive GFP probes of presynaptic activity, are presented and compared with Sapphire, a neutral phenol GFP mutant. Molecular dynamics have been characterized using fluorescence correlation spectroscopy (FCS) and time-correlated single-photon counting (TCSPC) as a function of pH, excitation wavelength (including 405 nm), detection wavelength, and illumination intensity. As a cellular pH indicator, Ecliptic (EcGFP) is particularly well-suited to the physiological pH range ($pK_a = 7.2 \pm 0.2$) compared with Sapphire (H9; $pK_a = 5.7 \pm 0.1$) and a number of other GFPs. However, both EcGFP and H9 exhibit complex, intensity- and wavelength-dependent partitioning between bright and dark EcGFP states, which may complicate their use in quantitative intracellular measurements. Furthermore, the protonation and deprotonation rate constants for the EcGFP chromophore may limit the ability to resolve pH jumps occurring on time scales faster than ∼0.5 ms. A proposed kinetic model of three-state transitions describes quantitatively the interstate conversion via reversible internal and external protonation. The excited neutral state fluorescence lifetime of EcGFP decays is significantly longer (i.e., larger fluorescence quantum yield) than most neutral GFPs, which can be exploited as a new spectral window in biological studies with multiple labels. The pH independence of the EcGFP neutral fluorescence lifetimes implies a ground-state interconversion mechanism for the observed fluorescence quenching in acidic environment.

1. Introduction

The prolific use of green fluorescent proteins (GFPs) in biochemistry and cell biology as multipurpose, noninvasive, genetically encoded reporters, has called for a vast variety of mutants with complex, yet fascinating, photophysical properties. Ranging from single molecules to whole mammalian organisms, the multitude of biological applications testifies to the tremendous potential that GFPs offer.[1,2] Optimal utilization of these molecular beacons in biology merits systematic spectroscopic and molecular dynamics studies.

The GFP chromophore exists in anionic (deprotonated) and neutral (protonated) forms, with ground-state populations that depend on the environmental acidity.[2] The interconversion of the ground-state populations occurs via a reversible protonation reaction with the buffer on submillisecond time scales.[3] Evidence for a decarboxylation of E222 immediately preceding chromophore deprotonation has been demonstrated by mass spectroscopy measurements.[4] Further, light-dependent fluorescence flicker on microsecond time scales[3,5,6] under intense laser illumination, and blinking of immobilized molecules due to optically induced switching at low intensities on ∼1 s time scales[7] have been reported.

The excited anionic state fluorescence lifetime of GFP is 2.8− to 3.7 ns, depending on mutation site and type.[6,8,9] On the other hand, the excited neutral state fluorescence decay is more complex and occurs on a much faster time scale of tens to hundreds of picoseconds.[6,8,9] Proton transfer (or internal proton displacement) also occurs on the excited-state potential energy surface (PES) with ∼15 ps time scale[10,11] with pH sensitivity in several newly developed, closely related green fluorescent protein mutants.[12]

The inherent pH sensitivity of GFPs and the power of genetic manipulation have been exploited to create a new class of mutants, the pHluorins, which are exceptionally pH sensitive in the physiological pH range ($pK_a \sim 7.1$).[13] Recent studies have focused on targeted properties such as new spectral windows, particularly with red-shifted emission,[8,14] and improved sensitivity to specific ion concentrations such as Ca^{2+},[15] Cl^-,[16] I^-, NO_3^-,[17] H^+,[13,18] membrane potential,[19,20] and refractive index.[21] Like other GFP mutants, the pHluorins have the potential to provide site-specific intracellular information about protein expression, trafficking,[22] and protein−protein interactions,[23] in addition to simultaneous pH readout in a microscopic environment. Furthermore, it has been established that pHluorins can be used in neuroscience,[13,24−26] secretion,[13,27] and mutagenesis studies.[19]

Ecliptic pHluorin (S147D/A206T/Q204T/S202F/N149Q/T161I; referred to as EcGFP hereafter) is particularly well-suited ($pK_a \sim 7.1$) to exocytosis from acidic compartments such as

* Corresponding author. Phone: 607-255-3331. Fax: 607-255-7658. E-mail: www2@cornell.edu.
‡ Department of Physics.
⊥ Current address: Laboratory for Cellular and Molecular Biophysics, National Institute of Child Health and Human Development, National Institutes of Health, Bethesda, MD 20892-1855.
† School of Applied & Engineering Physics.
§ Current address: Department of Bioengineering, Pennsylvania State University, 231 Hallowell Building, University Park, PA 16802.
# These authors contributed equally.

10.1021/jp0362077 CCC: $27.50
Published on Web 04/23/2004

secretory vesicles. Ratiometric pHluorin (S202H/E132D/S147E/N149L/N164I/K166Q/I167V/ R168H/L220F; referred to as RaGFP hereafter) exhibits an excitation spectrum with two conspicuous peaks with opposite pH-dependent behavior. Following the excitation of each peak, the ratio of emission at 504 nm can be calibrated for sensitive pH measurement inside intracellular compartments.[13]

In this report, we present a comprehensive analysis of the fluorescence photoconversion kinetics in pHluorins as a function of pH and light intensity. The illumination intensity-dependent kinetics are of particular concern in quantitative biological applications such as single-molecule fluorescence imaging. For significant comparison, we also report results on Sapphire (S202F/T203I, referred to as H9 hereafter),[2] a particular GFP mutant with dominant neutral state absorption, but with different pH-dependent properties. Various spectroscopic techniques enable us to elucidate the photophysics of the pHluorins and H9 in both wavelength and time (picosecond to microsecond) domains. The results are discussed within the context of environmental acidity, mutations, and a simple model with one anionic and two neutral forms of the chromophore, which can be interconverted by external and internal protonation.

2. Methods

2.1. Sample Preparation. Fluorescent proteins were used as received from J. Rothman (Memorial Sloane Kettering Cancer Center; EcGFP and RaGFP) and R. Tsien (University of California San Diego; H9). S65T and enhanced GFP mutants (BD-Biosciences/Clontech, Palo Alto, CA) were used as received in 100 mM potassium phosphate buffers of known pH values. Carboxyfluorescein (9936; Eastman Kodak, Rochester, NY) and rhodamine green (R-6107; Molecular Probes, Eugene, OR) were dissolved in distilled high-purity (HPLC) water and used in control experiments. Samples were prepared just before the measurements. Absorption spectra were measured in a diode-array spectrophotometer (8502A; Hewlett-Packard, Palo Alto, CA) while the steady-state fluorescence excitation and emission spectra were recorded with a PC-controlled fluorometer (101; Photon Technology International, South Brunswick, NJ).

2.2. Fluorescence Correlation Spectroscopy (FCS). The experimental FCS setup is described in detail elsewhere.[8] Briefly, a pulsed (100 fs at 80 MHz repetition rate) infrared laser beam from a mode-locked Ti:Sapphire laser (Tsunami; Spectra Physics, Mountain View, CA) is frequency doubled to generate either 405 or 475 nm. Then, the second harmonic is steered into the back aperture of an underfilled objective (60× 1.15 NA, infinity corrected; Olympus, Melville, NY), using a dichroic mirror (490LP), then focused into the sample (concentration ~1−10 nM in a 200 μL deep-well glass slide). The filtered (525/50 nm and 530/50 nm) epi-fluorescence is collected through the same objective and then focused onto a confocal aperture (an optical fiber of 50 or 100 μm nominal core diameter) before being detected by an avalanche photodiode (SPCM-AQ; EG&G, Gaithersburg, MD). The signal is then processed with a PC correlator card (5000; ALV Inc., Hamburg, Germany) to calculate an autocorrelation curve $G(\tau)$, which is usually fitted appropriately with the following function:[5,28]

$$G(\tau) = N^{-1}[1 + \tau/\tau_D]^{-1}[1 + \tau/\omega^2\tau_D]^{-0.5}\prod_{i=1}^{m}\{[1 - f_i + f_i\, e^{-\tau/\tau_i}]/[1 - f_i]\} \quad (1)$$

where τ_D is the characteristic diffusion time of a molecule residing in a Gaussian observation volume with axial (z_0) to lateral (r_0) dimension ratio $\omega = z_0/r_0$. The mean number of fluorescent molecules is N, while f_i is the fraction of molecules that reside in a dark state for characteristic time (τ_i). The exponential decay terms describe the kinetics of m independent transitions between states of different spectroscopic properties.[3,29] For diffusion alone, $f_i = 0$ as in our control experiments on rhodamine green (RG) under low intensity with $\tau_D \sim 0.6-0.8$ ms and $\omega < 15$, which ensures a Gaussian observation volume and provides the basis for correct analysis of chemical and diffusion kinetics.[30] The background fluorescence from buffer made with high-purity water was negligible. At a given illumination wavelength (λ_x) and intensity (I), the excitation rate (k_x) was estimated using $k_x(\lambda_x) = \sigma(\lambda_x)I(\lambda_x)$, with the most uncertainty due to the calculated excitation intensity.[30] Generally, twenty runs (of 30 or 60 s each) are averaged to obtain a $G(\tau)$ with good signal-to-noise ratio.

2.3. Time-Correlated Single-Photon Counting (TCSPC). The experimental setup for TCSPC is described in detail elsewhere.[8] Briefly, frequency-doubled femtosecond IR pulses (see the FCS section) were pulse-picked (4 MHz repetition rate) by a Pockel's cell and focused into the sample (concentration ~1−5 μM in a 3 mm × 3 mm quartz cuvette). Right-angle fluorescence was imaged onto the entrance slit of a spectrometer (270M; Instruments S. A., Inc., Spex division, Edison, NJ) with a microchannel plate (MCP) photomultiplier (R3809U059; Hamamatsu Corp. USA, Bridgewater, NJ) mounted on the exit slit. The MCP signal was then amplified and processed by a PC-card-controlled single-photon counting module (SPC-430; Becker & Hickl, Germany). The instrumental response function (fwhm ~ 60 ps) was measured regularly for deconvolution, yielding an estimated temporal resolution of ~15 ps. Decays were least-squares fitted using a routine based on Marquardt's algorithm.[6,31,32] Magic angle detection (54.7° relative to the excitation polarization) was used to eliminate molecular rotational effects. The average fluorescence lifetime is defined[6] as $\langle\tau_{fl}\rangle = \Sigma_i\, a_i\tau_i$, where the time constant τ_i for the ith decay component is weighted by its fractional contribution a_i to the overall fluorescence decay.

3. Results

3.1. Steady-State Spectroscopy. Figure 1 (top) shows the absorption and emission spectra of EcGFP, RaGFP, and H9 at low and high pH. The maximum absorption in both EcGFP (at ~397 nm) and H9 (at ~396 nm) is assigned to the neutral state transition of the chromophore, similar to other neutral GFPs.[2,6] The molar extinction coefficient (ϵ) of H9[2] is ~2.0×10^4 M^{-1} cm^{-1} at 399 nm and $\epsilon = (2.7 \pm 0.3) \times 10^4$ M^{-1} cm^{-1} was estimated for EcGFP at 405 nm, with weak absorption around 475 ± 25 nm. The neutral band is relatively pH independent in contrast with the anionic absorption, which is ~17% and ~4% of the main peak of EcGFP and H9 (at high pH), respectively (see Table 1). At low pH, the anionic state absorption in EcGFP diminishes, while it increases by ~12% of the neutral absorption band (at 398 nm) in H9 at pH 5. RaGFP (high pH) exhibits two pH-dependent absorption bands (~396 nm with $\epsilon \sim 58 \times 10^3$ M^{-1} cm^{-1} and ~476 nm with $\epsilon \sim 38 \times 10^3$ M^{-1} cm^{-1}).

The fluorescence emission (Figure 1, bottom) of EcGFP is significantly dependent on the excitation wavelength (405 and 475 nm) with an emission shoulder (at ~430−500 nm) that is pH independent (Figure 1K). The anionic emission band is minimal at low pH (5.5), while the neutral state emission and absorption remain unchanged. Thus, EcGFP provides a unique opportunity to investigate the neutral state transition in the presence of a negligible population of anionic chromophores.

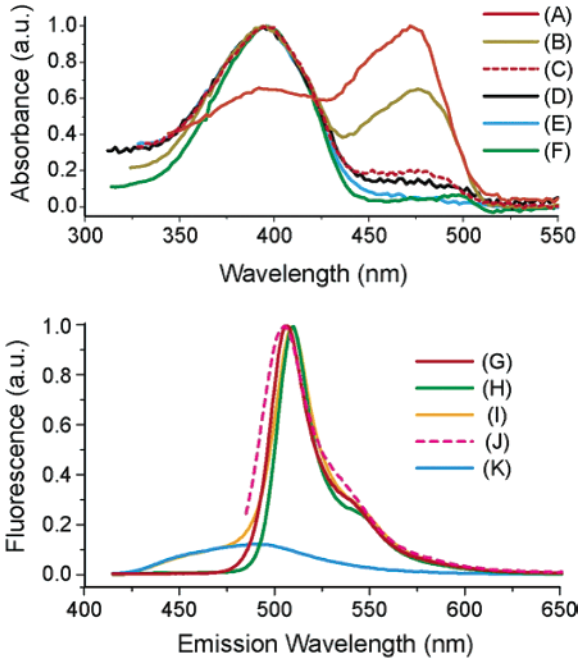

Figure 1. Steady-state spectroscopy of GFPs reveals pH, wavelength, and mutation dependence. (Top) Absorption spectra of (A) RaGFP pHluorin at pH 6.1, (B) RaGFP at pH 7.5, (C) EcGFP pHluorin at pH 7.4, (D) H9 at pH 5, (E) EcGFP at pH 5.5, and (F) H9 at pH 9. (Bottom) Fluorescence emission spectra. (G) RaGFP excited at 405 nm and pH 7.5. (H) H9 excited at 405 nm and pH 9. (I−K) EcGFP: at pH 7.4 under 405-nm (I) and 475-nm excitation (J); at pH 5.5 under 405 nm (K). Extinction coefficients are given in the text. Curves (I) and (K) were not scaled relative to each other. Black arrow emphasizes significant emission of EcGFP in the wavelength range of 430−480 nm.

3.2. Time-Resolved Fluorescence Decays. Selective excitation and detection of the neutral and anionic chromophore fluorescence facilitates monitoring the temporal evolution of the excited-state population of each species. On the basis of the steady-state spectroscopy of GFPs, the neutral state can be excited at ∼400 nm and detected selectively at $\lambda_{fl} \sim 460$ nm, which is quite distinct from the ionic state transition ($\lambda_x \sim 475$ nm and $\lambda_{fl} > 510$ nm). The measured fluorescence decays confirm these two distinct regimes as shown below.

3.2.1. Anionic State Transition (475−490 nm Excitation). The first excited anionic state fluorescence of EcGFP decays as a monoexponential with a lifetime $\tau_{fl} = 3.15 \pm 0.06$ ns and $\chi^2 = 1.02$ (Figure 2A), similar to wild-type (wt)-GFP.[6] The lifetime of H9 exciting at 490 nm was $\tau_{fl} = 3.16$ ns ($\chi^2 = 1.02$) at pH 7.4 and did not change significantly at pH 4.9. The anionic RaGFP fluorescence lifetime is slightly shorter ($\tau_{fl} \sim 2.98 \pm 0.10$ ns) and is independent of both excitation wavelength (400−490 nm) and pH ($\tau_{fl} = 2.89 \pm 0.01$ ns at pH 5.5 and 475-nm excitation). Similar results were measured for S65T ($\tau = 2.98 \pm 0.02$ ns) and enhanced GFP (EGFP: F64L/S65T with $\tau_{fl} = 2.80 \pm 0.04$ ns),[6] which belong to the phenolate anion class of GFPs.[2] The enhancement of the anionic-to-neutral population ratio (∼2:1)[33] in RaGFP can be attributed to the I167V mutation. For the same reason, RaGFP properties are considered as intermediate between the two wild-type and phenolate anion classes.

3.2.2. Intrinsically Neutral State Transition (405-nm Excitation). In both the EcGFP and H9 mutants, the excited neutral state decays as a multiexponential with mainly ultrafast time constants (Figure 2). The neutral form of the GFP mutants can be excited and detected effectively at 398 and 460 nm, respectively (Figure 1).[2,6,8] Under 405-nm illumination, the 460-nm fluorescence of EcGFP (pH 7.4) decays as a multiexponential with $\tau_1 = 1.28$ ns ($a_1 = 31\%$), $\tau_2 = 510$ ps ($a_2 = 42\%$), $\tau_3 = 66$ ps ($a_3 = 27\%$), and $\chi^2 = 1.13$, which yields an average lifetime $\langle\tau_{fl}\rangle \sim 629$ ps (Figure 2C). A similar trend (See Figure 2D: $\tau_1 = 27$ ps, $a_1 = 78\%$, $\tau_2 = 380$ ps, $a_2 = 15\%$, $\tau_3 = 1.4$ ns, $a_3 = 7\%$, and $\chi^2 = 1.98$) is also observed for H9 (pH 9.0) but with $\langle\tau_{fl}\rangle \sim 181$ ps, which is much faster than that of EcGFP.

Minor changes in the neutral fluorescence decay parameters were observed in EcGFP at pH 5.5 (See Figure 2B: $\tau_1 = 1.29$ ns ($a_1 = 37\%$), $\tau_2 = 586$ ps ($a_2 = 44\%$), $\tau_3 = 221$ ps ($a_3 = 19\%$), and $\chi^2 = 0.97$) with $\langle\tau_{fl}\rangle \sim 777$ ps (i.e., ∼23% slower than the pH 7.4 decay) compared with $\tau_1 = 42$ ps ($a_1 = 58\%$), $\tau_2 = 430$ ps ($a_2 = 30\%$), $\tau_3 = 1.38$ ns ($a_3 = 12\%$), and $\chi^2 = 1.17$ for H9 where $\langle\tau_{fl}\rangle \sim 280$ ps (i.e., about 2 times slower than the decay at pH 9). Figure 2E depicts the average fluorescence lifetime of H9, excited at 405 nm, as a function of the detection wavelength, which indicates two distinctive regimes that can be assigned to the neutral ($\langle\tau_{fl}\rangle \sim 300-500$ ps) and anionic ($\langle\tau_{fl}\rangle \sim 3.14$ ns) state transitions.

3.2.3. Excited-State Proton Transfer. Following 405-nm excitation of EcGFP, the intrinsically neutral excited-state fluorescence (460 ± 15 nm) decays as a multiexponential (Figure 2). Under the same excitation conditions, the anionic state fluorescence (at 510 nm) builds up on a ∼15 ps time scale ($a_1 = -44\%$) followed by a biexponential fluorescence decay with $\tau_1 = 2.82$ ns ($a_2 = 40\%$), $\tau_3 = 480$ ps, $a_2 = 16\%$, $\chi^2 = 1.15$ (Figure 3). Fitting without a fluorescence buildup (i.e., a rise) left the fitting residual significantly modulated (see Figure 3, C and D). The rise time of the 510-nm fluorescence is attributed to excited-state proton transfer (ESPT).[10,11]

3.3. Fluorescence Fluctuation Autocorrelation. Using FCS at low illumination intensity (below saturation), the estimated diffusion coefficients of EcGFP and H9 (high pH) are $(9 \pm 1) \times 10^{-11}$ m^2/s and $(8 \pm 1) \times 10^{-11}$ m^2/s, respectively. These values are in good agreement with the literature for wt-GFP and GFP mutants such as EGFP and S65T.[34−36] Furthermore, the correlation function of both H9 and EcGFP reveals two fluorescence flickering processes (Figures 4 and 5). One of these processes is pH dependent and the other is dependent only on the excitation light intensity. Light- and pH-dependent flicker have been observed in other GFP mutants [3,5,8] but the flicker in EcGFP and RaGFP is distinct because of the population partitioning between fluorescent and nonfluorescent states (see below).

Under intense illumination, fluorescence saturation is observed and light-driven flicker (i.e., photoconversion), photobleaching, as well as intersystem crossing become significant. In a two-level system, the actual saturation intensity threshold can be calculated, using the excited state lifetime and excitation cross-section ($I = 1/\tau_{fl}\sigma$) of a given fluorophore. However, the apparent experimental intensity threshold for saturation, where the fluorescence count rate per molecule becomes constant, is 2−3 times lower than the calculated value for the two-level system. This implies that the triplet state population must be included (work in progress) especially at high illumination intensities. For example, the EcGFP fluorescence becomes nonlinear at excitation rate $k_x \sim 1.0 \times 10^6$ and $k_x \sim 0.5 \times 10^6$ s^{-1} under 405- and 488-nm excitation, respectively. On the other hand, the apparent saturation of H9 fluorescence at excitation rate $k_x \sim 0.8 \times 10^6$ s^{-1} (high pH) is basically excitation wavelength independent. As shown below, we used FCS to quantify the kinetics of the two flicker processes, including photoconversion.

3.3.1 pH-Dependent Fluctuation Autocorrelation. As mentioned above, the anionic state transition of GFPs can be excited

TABLE 1: Intensity-Dependent Flicker Parameters versus Excitation Wavelength and pH

	excitation conditions			pH-independent flicker		pH-dependent flicker	
molecule	λ_x (nm)	pH	$\epsilon \times 10^3$ (M^{-1} cm^{-1})	$\phi_i \times 10^{-3}$	k_{0i} (kHz)	$\phi_x \times 10^{-3}$	k_p (kHz)
EcGFP	488	7.4	4 ± 2[a]	50[a]	<1.0	0.7[b]	0.7
	405	5.5	30	3	6 ± 1	~10[b]	120
	405	7.4	27	10 ± 5	<1.0		
H9	488	9	3 ± 2[a]	8 ± 3	~0.3		
	488	5.2	2.4 ± 2[a]	5 ± 3	1.5 ± 1.2	~0	170
	405	5.2	20[c]	190 ± 30	10 ± 3	~100[b]	220
	405	9	20[c]	5 ± 3	<1.0	~10[b]	80
RaGFP	488	7.5	32	0.5	1.7 ± 1.0		

[a] The small extinction coefficients ϵ are very uncertain; because ϵ is used to calculate k_x, a larger value would mean a smaller quantum yield (ϕ_i) value. The model predicts that only half of the molecules will be in the anionic state at pH 7.4, in which case the extinction coefficient would be twice as large and ϕ_i twice as small. [b] Quantum yield very uncertain; rate is fast and relatively intensity independent. [c] Tsien, 1998.[2]

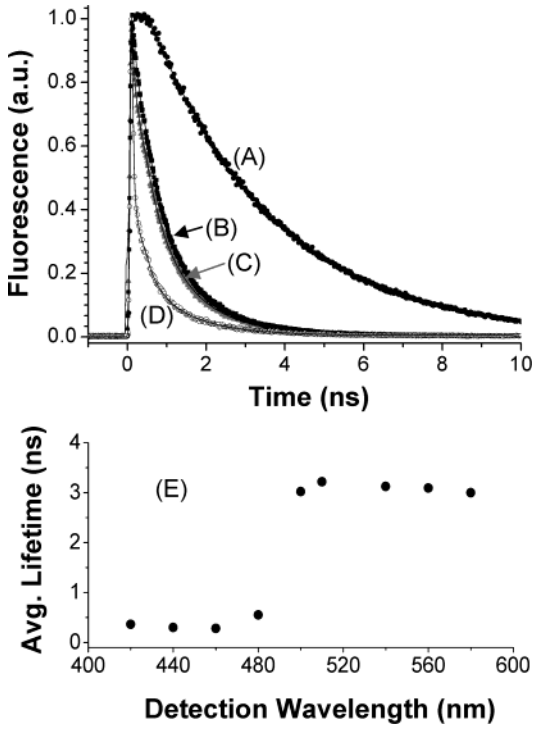

Figure 2. The fluorescence decays of the excited neutral and anionic states occur on distinctively different time scales. (Top) Fluorescence decays of EcGFP and H9 (points) with accompanying fits (lines). (A) EcGFP with $\lambda_x = 475$ nm, $\lambda_d = 570$ nm, pH 8.3, and monoexponential fit with $\tau = 3.11$ ns, $\chi^2 = 1.17$. (B) EcGFP with $\lambda_x = 405$ nm, $\lambda_d = 460$ nm, pH 5.5 and multiexponential fit. (C) EcGFP with $\lambda_x = 405$ nm, $\lambda_d = 460$ nm, pH 7.4 and multiexponential fit. (D) H9 with $\lambda_x = 405$ nm, $\lambda_d = 460$ nm, pH 9 and multiexponential fit. See text for multiexponential decay fitting parameters. (Bottom) Detection-wavelength dependence of 405-nm excited average fluorescence lifetime of H9 at pH 9 (filled circles).

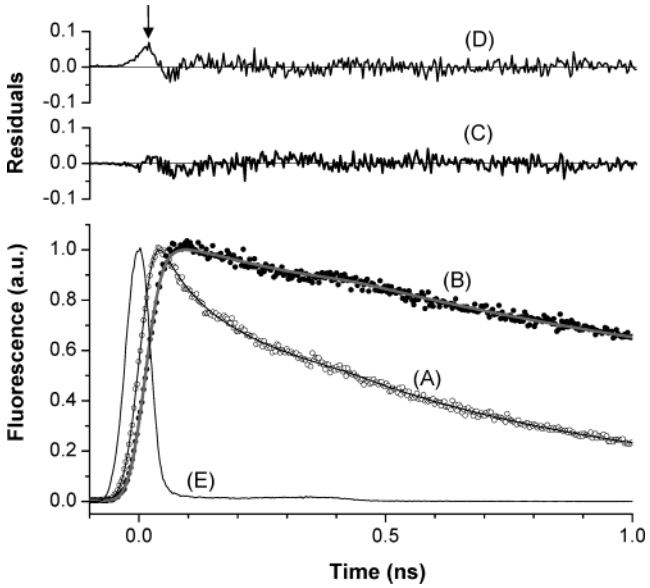

Figure 3. Ultrafast excited-state proton transfer competes with the neutral excited-state fluorescence decay in EcGFP (high pH), excited at 405 nm. (A) The instantaneously populated (within fwhm of the response function) neutral excited-state fluorescence at 450 ± 5 nm decays as a triexponential with $\tau_1 = 1.08$ ns (30%), $\tau_2 = 410$ ps (37%), $\tau_3 = 52$ ps (33%), $\chi^2 = 0.92$. (B) The detected fluorescence at 570 ± 5 nm rises on a time scale of ~15 ps (amplitude of −44%) while decaying with two components: $\tau_1 = 2.82$ ns (40%), $\tau_2 = 480$ ps (16%), and $\chi^2 = 1.15$. (C) The fitting residuals for the 570-nm (B) fluorescence decays with a rise and (D) without rise. (E) Measured detector response.

at 475 nm. The fluorescence correlation curves of anionic EcGFP and H9 ($\lambda_x = 488$ nm; $\lambda_{fl} = 525 \pm 25$ nm) are shown in Figure 4 (top), where eq 1 was used to fit the experimental data (Figure 4, bottom) and to estimate the flicker rate ($k_p = 1/\tau_p$) as a function of pH. The autocorrelation of anionic H9 fluorescence (525 ± 25 nm, high pH) is also shown for comparison (Figure 4) and is distinctively different at low pH (5.2). The estimated flicker time of H9 is $\tau_p \sim 5.3$ μs with a large dark molecular fraction (~75%).

3.3.2. Excitation-Dependent Fluctuation Autocorrelation (A): Anionic State Transition (475-nm Excitation). All GFP mutants (at high pH) studied here exhibit a light-driven fluorescence flicker at 488-nm excitation (Figure 5). The fluorescence flickering rate (k_i) increases linearly (Figure 5; top) with the excitation rate (k_x). (Flicker rates for RaGFP are plotted at 0.2 times the actual excitation rate for illustrative purposes.) The flicker quantum yield[28] (ϕ_i) of anionic EcGFP (~ 5×10^{-2}), H9 (8×10^{-3}) and RaGFP (0.5×10^{-3}) are summarized in Table 1. The anionic chromophore is the dominant fluorescence emitter under 488-nm excitation and therefore is involved in the light-driven flicker. However, because the light-dependent pH-independent flicker is distinct from the pH-dependent flicker, an additional chemically distinct transition (to an externally protonated dark state, heuristically named the "quasi-neutral" state), must be involved.

(B): Intrinsically Neutral State Transition (405-nm Excitation). As mentioned above, the steady state spectroscopy and time-resolved fluorescence indicate that the neutral state transition is distinct and can be excited at 395-nm. As a result, FCS measurements at 405 nm should allow elucidation of the role of neutral state transition(s) in the photoconversion and flickering processes in GFPs. The light-dependent flicker rate depends linearly on the 405-nm excitation rate below fluorescence saturation (Figure 5). The flicker quantum yield (ϕ_i) and dark

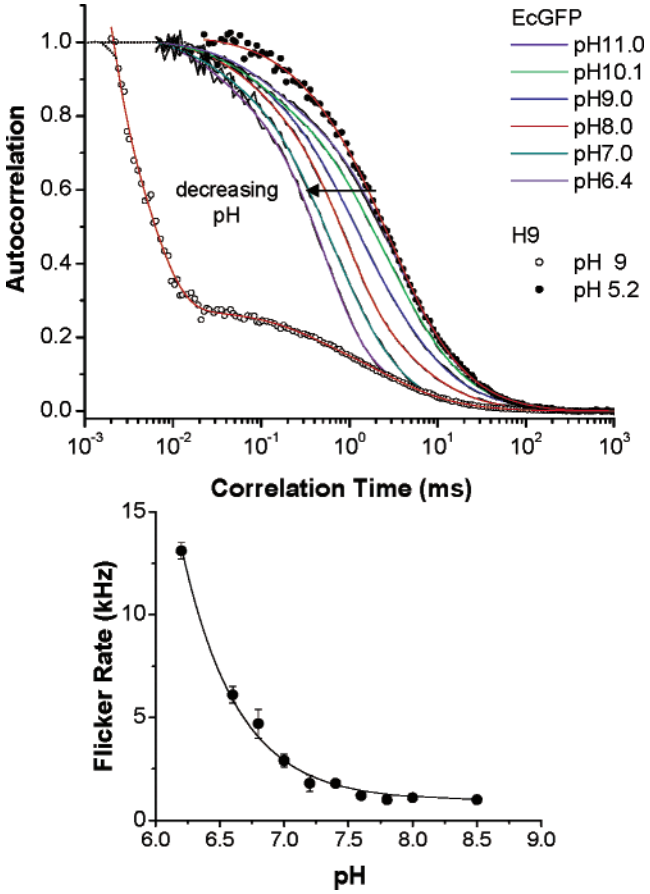

Figure 4. The dynamics of ground-state partitioning between neutral and anionic GFPs, based on the environmental acidity, can be monitored using FCS. (Top) pH-dependent FCS correlation curves of EcGFP (excited at 488 nm), where the intermediate curves from right to left are measured at pH 11, 10.1, 9, 8, 7, and 6.4. The correlation curves of H9 are also shown for comparison at pH 5.2 (leftmost curve, open circles) and pH 9 (right, filled circles). The solid lines represent the fitting curves. (Bottom) The pH dependence of the fluorescence flicker rate (solid black circles) in EcGFP, excited at 488 nm under low illumination, and the least-squares fit (solid line) yield p$K_a \sim 7.2$.

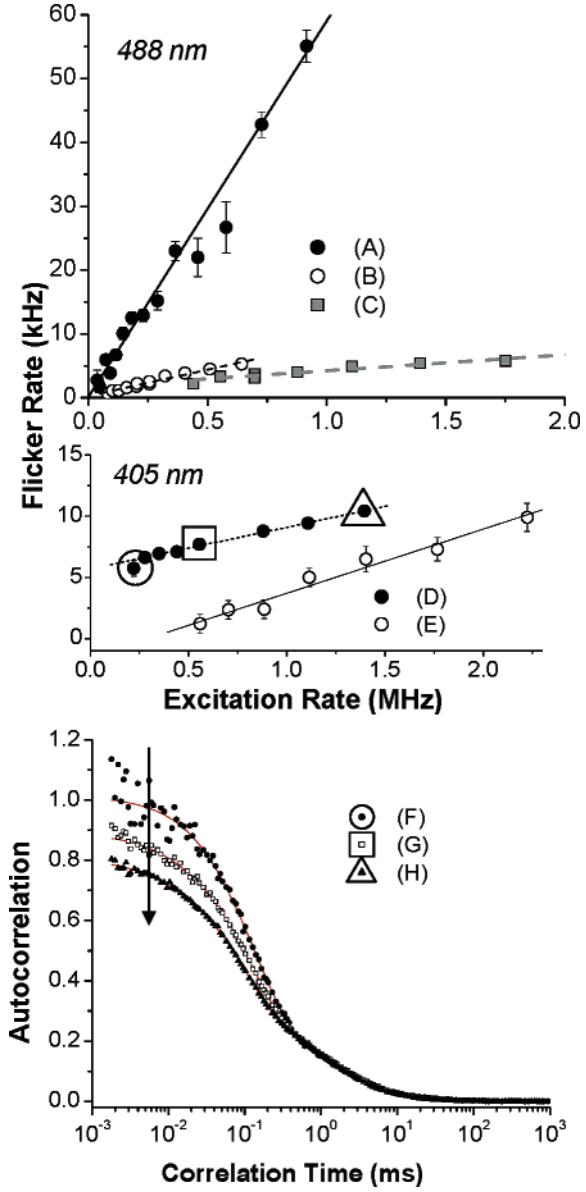

Figure 5. Light-dependent fluorescence flicker is revealed by FCS studies on EcGFP, H9, and RaGFP as a function of excitation wavelength. (Top) The dependence of the fluorescence flicker rate constant on the excitation rate (488 nm) is shown for EcGFP (A), H9 (B), and RaGFP (C) mutants (high pH). The plotted excitation rate for RaGFP is shown at 0.2 times the measured values for illustrative purposes. The estimated flicker quantum yields from the slopes are $\phi \sim 5 \times 10^{-2}$ (EcGFP; solid black line), $\phi \sim 8 \times 10^{-3}$ (H9; dashed black line), and $\phi \sim 0.5 \times 10^{-3}$ (RaGFP; dashed heavy gray line). The rate appears to extrapolate to nearly zero at very low intensity. (Middle) Light-dependent flicker in EcGFP (p$K_a \sim 7.2$) illuminated at 405 nm. (D) The observed EcGFP (pH 5.5) fluorescence flicker, as a function of the excitation rate, yields $\phi \sim 3 \times 10^{-3}$ (dashed black line) and intercept (6 ± 1 kHz) which are different than the values at pH 7.4 (E): intercept near zero and $\phi \sim 10 \times 10^{-3}$. (Bottom) Autocorrelation of EcGFP excited at 405 nm at pH 7.4 at illumination intensities corresponding to points in plot of part D: (F) point in circle (G) point in box. (H) point in triangle. Solid lines are fits using eq 1 with diffusion plus one chemical kinetic factor. Dotted lines are fits using eq 1 with diffusion kinetics only. Arrow shows direction of increasing illumination intensity.

flicker rate (k_{0i}; flicker rate extrapolated to zero excitation intensity) are summarized in Table 1. The values of k_{0i} and ϕ_i of EcGFP depend on the pH (Figure 5) with $\phi_i \sim 3 \times 10^{-3}$, $k_{0i} = (6.1 \pm 0.7)$ kHz (at pH 5.5) and $\phi_i = (10 \pm 5) \times 10^{-3}$, $k_{0i} = (0.9 \pm 0.9)$ kHz (at pH 7.4). The differences in k_{0i} imply that the energy barriers separating the neutral and anionic ground-state PESs depend on the external pH. The magnitude of ϕ is smaller than the literature value for wt-GFP ($\phi_i = 0.03$) when excited at 254 nm.[4]

The dark fraction of the GFP population is strongly dependent on 405-nm intensity, which is in contrast with the observed constant fraction at 488-nm excitation. The neutral state transition of EcGFP (low pH) can be investigated selectively, since the anionic state absorption is negligible (Figure 1). The dark fraction of EcGFP (low pH) decreases with k_x (Figure 7), similar to H9 (high pH) anionic emission (500−550 nm). The results suggest that ground-state population partitioning, between the bright and dark states, is also dependent on light intensity. This observation supports the proposed kinetic model describing fluorescence flicker (see below).

4. Discussion

4.1. Molecular Classification of GFP Mutations. Tsien[2] classified GFP mutants in terms of the molecular structure of the embodied chromophore and its mutations. There is a correlation between the structure of each class and the corresponding fluorescence properties and thermodynamics. For example, the mutation of S65 by Y, G, A, or L has been shown to enhance the anionic chromophore population with a correlated reduction of the neutral population.[2] The large number of

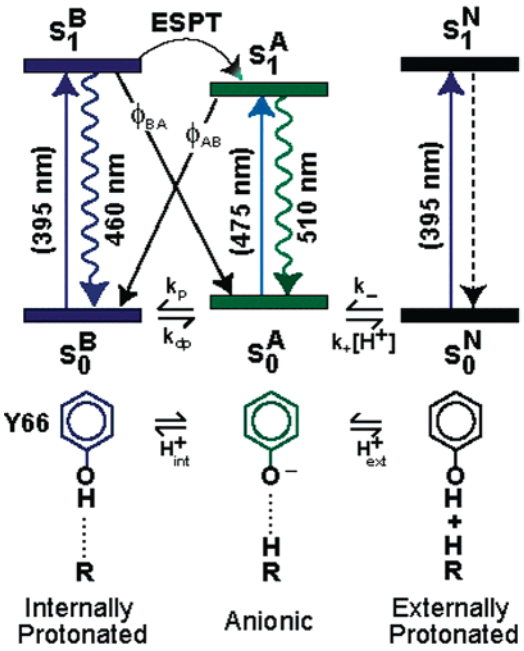

Figure 6. Schematic kinetic model demonstrates both light- and pH-induced interconversion between different electronic states in GFP mutants. The intrinsically protonated electronic transition ($S_0^B \rightarrow S_1^B$) absorbs maximally at 396 nm and corresponds to the AH-state of the chromophore by Haupts et al.,[3] while the anionic transition ($S_0^A \rightarrow S_1^A$) absorbs maximally at 475 nm, depending on sequence mutations. The corresponding fluorescence emission is also shown and is dependent on mutation site/type (especially for the anionic state). The externally protonated state transition ($S_0^N \rightarrow S_1^N$) is also shown (which corresponds to the AH'-state of the chromophore by Haupts et al.[3]) and is heuristically named the "quasi-neutral" state, due to the fact that external proton binding to the embodied chromophore is a reversible process. Rate constants for the interconversion among these states are also shown, e.g., internal protonation (k_{ip}) and deprotonation (k_{id}) as well as external protonation (k_+) and deprotonation (k_-). The diagonal gray arrows represent the quantum yield (ϕ) for photoconversion between different states. While believed unlikely, direct conversion between N and B states cannot be ruled out. The corresponding chromophore structure (only the Y66 moiety and the nearest residue R in its vicinity) for each state transition is also shown (bottom).

pHluorin mutations makes it difficult to link the observed fluorescence and thermodynamics variations to site-specific mutations. However, five of the six mutations in EcGFP are adjacent to three residues (namely H148, T203, and S205) which are believed to play a crucial role in stabilizing the anionic form of the chromophore.[2] The mutation S147 → N, a pH-sensitive charged residue with a proton-binding site (typical p$K_a \sim 4.5$) next to H148, could conceivably increase the chromophore pH sensitivity. Mutations also introduce changes in the side chains and, therefore, structural rearrangements of the H148, T203, and S205 residues relative to Y66. This rearrangement might disrupt the anionic chromophore stabilization.

Neither H9 nor EcGFP contains a mutation at the 65 residue, which could explain their dominant neutral character (maximum absorption at ~396−397 nm). The presence of S65 allows a hydrogen bond to form with E222 and gives the chromophore an anionic character. Accordingly, both mutants belong to the wt-GFP and neutral phenol class, respectively.[2] On the other hand, the I167V mutation[33] enhances the anionic RaGFP population, which should also decrease the chromophore affinity for protons. In contrast, the neutral H9 population enhancement is likely due to the T203I mutation, which presumably prevents solvation of the chromophore anion because of the absence of

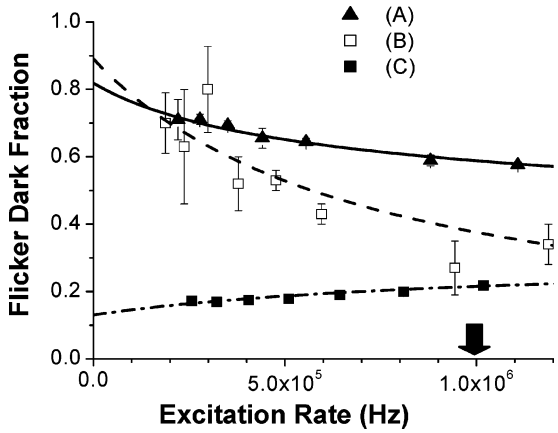

Figure 7. Quantitative analysis of the flicker dark fraction in GFPs as a function of excitation wavelength and intensity supports our interconversion model (see Appendix). (A) The amplitude fraction of dark EcGFP at pH 5.5 (triangles) declines monotonically with illumination (405 nm) excitation rate. (B) Similar results for H9 (pH 9 and 405 nm) are also shown (open squares) with best fit (dash dot line). (C) The excitation rate dependence of the dark faction of H9 at pH 9 excited at 488 nm (filled squares) is also shown for comparison. Equations A10−A12 based on the three-state model were fitted (lines) to the experimental data. The black arrow indicates approximately the excitation intensity above which fluorescence saturation was observed.

the hydroxyl group from T203.[2] However, a weak anionic state population is observed in the H9 absorbance at both high and low pH. Interestingly, the relative fraction of the anionic state absorption (~475 nm) is higher in an acidic environment.

4.2. Distinct Excited-State Dynamics of Neutral and Anionic GFPs. Previously, acid quenching of GFP fluorescence has been often attributed to a reduction in fluorescence quantum yield (Φ_{fl}) at low pH.[37] This argument suggests a reduction of the excited-state fluorescence lifetime at low pH (assuming that the radiative rate, k_{rad}, is constant). The fluorescence quantum yield is a function of both the radiative (k_{rad}) and nonradiative (k_{nr}) rate constants, where $\Phi_{fl} = k_{rad}/k_{fl} = k_{rad}\tau_{fl}$ and $k_{fl} = \tau_{fl}^{-1} = k_{rad} + k_{nr}$. However, the first excited anionic state fluorescence of both RaGFP and H9 decays are almost independent of pH (9.0 to 5.0), in agreement with previous studies on S65T (data not shown) and other GFP mutants.[6] Furthermore, the environmental pH effects are negligible on the maximum absorption and emission wavelengths (and, therefore, the radiative rate constant). Accordingly, the pH sensitivity of GFP absorption must be due to the ground-state population partitioning between neutral and anionic states rather than a reduction of the fluorescence quantum yield. This would also explain the pH dependence of EcGFP and H9 absorption. Such ground-state partitioning must take place on slower time scales compared with the excited anionic state lifetime (~2.8−3.1 ns) as previously reported for EGFP.[6]

Furthermore, the estimated radiative lifetimes are ~4.1 ns (wt-GFP), ~4.7 ns (S65T), ~4.8 ns (EGFP),[6] and ~5.2 ns (H9) based on the previously published quantum yield of wt-GFP (0.79), S65T (0.64), EGFP (0.6), and H9 (0.6)[2]. The nonradiative rate $k_{nr} \sim 1.3 \times 10^8\ s^{-1}$ for H9 fits nicely between EGFP ($\sim 1.5 \times 10^8\ s^{-1}$), GFP-S65T ($\sim 1.2 \times 10^8\ s^{-1}$), and the parent wt-GFP ($\sim 0.7 \times 10^8\ s^{-1}$). Thus, whether a mutation increases the fraction of molecules in the neutral state (i.e., H9) or the anionic state (EGFP and S65T), the nonradiative decay rate from the anionic state is increased relative to wt-GFP.

These results provide a new perspective for understanding FCS results according to the proposed kinetic model (see below). When such conversion occurs on the ground-state PES via

external proton exchange with the surrounding buffer, fluorescence flicker between the neutral and anionic species takes place, as observed by FCS.[3] Multiexponential fluorescence decay is typical of neutral GFPs,[6,8−11,38,39] due to a heterogeneous ground-state population (i.e., multiple conformers/states of the chromophore), as depicted in the proposed kinetic model (see below) which accounts for the observed FCS results.

4.3. Ultrafast Excited-State Proton Transfer. An internal photoconversion between the neutral and anionic GFP mutants has been proposed to occur on the excited-state PES by a proton transfer mechanism (ESPT).[10,11] The ESPT rate can be manipulated by the environmental pH as well as site-specific mutations.[40] The ESPT takes place on picosecond time scales and enhances the Stokes' shift in aequorin fluorescence.[41,42] The excited neutral state (λ_x = 405 nm) fluorescence (λ_{fl} = 475 nm) decays as a multiexponential with a long decay component that is fairly similar to the excited anionic state lifetime, possibly because of direct excitation of the anionic ground state. However, the anionic-state fluorescence (515 nm) builds up on a time scale (∼15 ps) possibly because of ESPT (Figure 2). In contrast to EcGFP, a delay of the anionic excited-state fluorescence was not observed in either H9 or RaGFP mutants under 405-nm excitation, with our experimental temporal resolution (∼15 ps). These results indicate that the excited intrinsically neutral state serves as a gateway to other excited states in EcGFP. Furthermore, the excited-state dynamics of the intrinsically neutral chromophores indicate efficient nonradiative channels under 396-nm illumination. As a result, it is expected that the fluorescence quantum yield would be wavelength dependent.[6] Photoconversion mechanisms might also include photoisomerization,[43,44] intramolecular energy redistribution between the neutral and anionic S_1-state vibrational manifolds, or decarboxylation of E222.[4] These processes constitute nonradiative pathways for the excited neutral state depopulation.

The absence of ESPT in RaGFP or H9 can be attributed to either a very efficient ESPT on a much faster time scale (compared with our temporal resolution) or an inhibition of the ESPT pathway. The anionic absorption of GFPs is weaker at 405 nm than at 488 nm (e.g., $\epsilon \sim 2.4 \times 10^3$ M^{-1} cm^{-1} for H9, Table 1, compared with $\epsilon \sim 5.6 \times 10^4$ M^{-1} cm^{-1} for EGFP[2]) and, therefore, a direct anionic excitation must be negligible at 405 nm. Thus, it seems plausible that ESPT may occur in RaGFP and H9 but not be resolvable by our methods.

Since ESPT competes with the excited internally protonated (B) state depopulation, a reduction in ESPT efficiency or rate would likely result in more efficient B-state fluorescence.[39] Lossau et al.[11] also observed ESPT in wt-GFP but not in a blue-shifted mutant (BFP11), due to the role of S205 in proton transfer between Y66 and E222 of the chromophore.[2] As a result, one would speculate that Q204T and A206T mutations (which are in the T203 vicinity) might also affect ESPT kinetics. The reason is that T203 stabilizes the negatively charged anionic phenolate by hydrogen bonding with its hydroxyl group[2,39] and may also play a role in ESPT. The relatively lower acidity of Y66 in the excited state could reduce the ESPT rate, resulting in more fluorescence emission from the neutral state.

4.4. Slow Protonation and Photoconversion of GFPs. The pH-dependent flicker rate is well-described by a reversible bimolecular reaction $A^- + H^+ \leftrightarrow N$ between the anionic (A) chromophore and a proton from the surrounding buffer to form the neutral (N) chromophore.[3] The external protonation flicker rate (k_P) is given by $k_P = \tau_P^{-1} \approx k_+ [H^+] + k_-$, where the forward (protonation, k_+) and reverse (deprotonation, k_-) reaction rate constants can be calculated from the measured flicker time at a known hydronium ion concentration, $[H^+]$. The kinetics of the proton transfer reaction, including the equilibrium constant ($K_e = k_+/k_-$), the pK_a, and the standard free reaction energy $\Delta_r G°$ can then be calculated. The dark population fraction undergoing pH-dependent flicker is defined as $F_P = [N]/([N] + [A]) = 1/(1 + k_-/k_+[H^+])$, where [N] and [A] are neutral and anionic chromophore concentrations, respectively. For a reversible bimolecular reaction,[3] the calculated pK_a values for RaGFP are slightly dependent on the illumination wavelength (6.4 ± 0.5 at 396 nm and 5.6 ± 0.5 at 476 nm), which can be attributed to differences between the pH sensitivity of the neutral and anionic chromophores, respectively. This state-specific pH sensitivity can be exploited to track intracellular pH changes.

The estimated protonation and deprotonation rate constants are $k_- = (1.1 \pm 0.5) \times 10^3$ s^{-1} and $k_+ = (1.9 \pm 0.2) \times 10^{10}$ s^{-1} M^{-1}, respectively, with insignificant differences at 10-fold higher intensity. Accordingly, the pK_a (7.2 ± 0.2) and the standard free energy $\Delta_r G°$ (−41.6 ± 0.9 kJ/mol) are calculated for the proton exchange reaction between the GFP mutants and the buffer. The pK_a is in a good agreement with the calculated value using the dark fraction populations (7.7 ± 0.4), as described above, and the previous steady-state measurements (pK_a = 7.2 ± 0.09).[25] However, the steady state measurements provide only the k_-/k_+ ratio, in contrast with the current FCS measurements, which provide a full description of the forward and reverse protonation reaction rates. Since molecules are most sensitive to acidity changes near the pK_a value, EcGFP is a particularly well-suited fluorescent marker near physiological pH.[13]

The autocorrelation curve of H9 fluorescence (525 ± 25 nm, high pH) also shows flicker (Figure 4) under 488-nm light. At low pH (5.2), the autocorrelation curve is distinctively different (Figure 4) with a flicker time constant $\tau_P \sim 5.3$ μs and a large dark molecular fraction (∼75%). Using these two parameters, the $k_- = (5.6 \pm 0.5) \times 10^4$ s^{-1} and $k_+ = (2.9 \pm 0.3) \times 10^{10}$ s^{-1} M^{-1}, with an estimated pK_a = 5.7 ± 0.1, which is in agreement with the previously reported ∼ 5.5 value.[37,45] For organelle-specific pH readout, H9 (p$K_a \sim 5.5$),[37,45] EGFP (p$K_a \sim 5.8$),[3,6] YFPs (p$K_a \sim 5.3$ and 5.2 for T203Y and T203F, respectively),[5] and citrine (p$K_a \sim 5.7$),[8] provide alternatives as pH indicators. Likewise, the free energy for the external protonation in EcGFP, $\Delta_r G° \sim 41.6 \pm 0.3$ kJ/mol at room temperature, is considerably larger than in EGFP ($\Delta_r G° \sim 33 \pm 1$ kJ/mol)[3] and citrine ($\Delta_r G° \sim 32.7 \pm 0.5$ kJ/mol).[8]

At zero-excitation rate, the extrapolated pH-independent flicker rate (k_{0i}) of EcGFP (at 405 nm) is nonzero (Table 1), which is in sharp contrast with FCS results on other GFPs[5,8] and DsRed.[8] For example, the flicker rate of RaGFP linearly extrapolates to $k_{0i} = 1.7 \pm 1.0$ kHz in the darkness (i.e., $k_x \rightarrow 0$), which suggests a spontaneous interconversion between the bright and dark states, on the ground-state PES, where k_{0i} is the sum of forward and backward reaction rates. The associated average dark population fraction is relatively constant under 488-nm illumination, with 9 ± 3% (EcGFP), 20 ± 5% (H9), and 40 ± 3% (RaGFP) at high pH, in agreement with previous studies on the anionic transitions in YFPs,[5,8] EGFP,[3] and DsRed.[8]

The flicker processes reported here are much faster than the slow blinking previously observed in wt-GFP, immobilized in polyacrylamide gels, which occurs on ∼1 s time scales.[7] Reversible photobleaching was also reported on even slower ($>10^2$ s) time scales with both excitation wavelength and intensity dependence.[7] According to our FCS results, reversible light-dependent partitioning between bright and dark states

occurs in EcGFP and H9 as well, but on much faster time scales ($\tau \sim 10^{-3}$ s). It is still an open question whether the flicker mechanisms underlying those observed kinetics (in different environments) are the same, and thus further investigation is merited. Novel photoactivated mutants, such as (PA)-GFP,[46] exploit a light-driven photoconversion mechanism like that described above for the T203H mutant. A slow spontaneous return and a negligible photoconversion quantum yield from the anionic state to the neutral state would explain the relatively long lifetime ($\gg$20 min)[46] of the bright (activated) population in PA-GFP. The relevant rate constants and quantum yields could be obtained directly by FCS measurements.

4.5. Kinetic Model for Interconversion in GFPs. Based on our findings and other works in the literature, we propose a kinetic model (shown schematically in Figure 6; the analysis is outlined in the Appendix) to account for both light- and pH-dependent interconversion between three molecular species. In addition to the anionic (A) and intrinsicially protonated (or neutral) state (B), we invoke a quasi-neutral state (N) which results from external proton binding to the anionic chromophore.[3]

One of the flicker processes is attributed to an external (pH-dependent) protonation of the bright anionic chromophore (A), which yields a neutral (N) dark state under 488-nm excitation, similar to other GFPs.[3,5,8] Furthermore, it is known by X-ray crystallography that external protonation results in significant structural rearrangement in S65T,[47,48] and in EGFP, as evinced from changes in the fluorescence anisotropy decay as a function of pH.[6] While the hydroxyl group in Y66 was proposed as the protonation site in EGFP,[3] other protonation sites have also been suggested.[44,49−52]

The second observed flicker process, which is not strongly pH dependent, presumably corresponds to light-driven transitions between the anionic (A) and an intrinsically neutral (B) state of the chromophore. These transitions are similar to those proposed for EGFP[3] and similar to T203Y/F,[5] except that the intensity dependence of the flicker fractions are now much more pronounced.[5,8] Our results do not prove or disprove the possibility of decarboxylation of E222 which might also be occurring as part of the photoconversion mechanism in pHluorins. The large, intensity-dependent fraction of molecules in dark states is consistent with the photoconversion mechanism previously reported for other GFPs using different experimental approaches.[4,7,53,54] Even when the anionic state transition is being excited ($\lambda_x \sim 488$ nm), there are indications that the neutral state of the chromophore can be partially populated.[8,55] One residue (H148) is proposed to donate a proton to the anionic Y66 moiety. Protonation of H148 in wt-GFP and S65T has been proposed[56] to play a role in solvent pH dependence.[47] However, while fluorescence flicker due to chromophore protonation is ubiquitous among GFPs, the kinetics of such processes are likely to be mutation type- and site-specific.

The average number of molecules that reside in dark states during the observation time (i.e., the dark fraction), is strongly dependent on the excitation intensity and wavelength in both EcGFP and H9 and can generally be well-described by the same model. The flicker rate is predicted to be linear with the excitation rate (Figure 5) with a slope equal to the quantum yield, while the zero-intensity intercept k_{0i} equals the sum of spontaneous forward and reverse reaction rates in the absence of light (see Table 1). The expressions A10−12 (see the Appendix) describe the flicker fraction dependence on the excitation rate using measured values for the external protonation rate constants (see above). The values of ϕ_{AN} and ϕ_{NA} were fixed to zero, since light dependence of external protonation was deemed unlikely because of the drastically different rate for external protonation compared with the excited-state fluorescence lifetime. The estimated internal protonation rate constants for the second process

$$(\mathrm{A} \underset{k_{id}}{\overset{k_{ip}}{\rightleftharpoons}} \mathrm{B})$$

using the measured flicker rate and fraction were used as fixed fitting parameters, and the results are shown in Table 2.

TABLE 2: Internal Deprotonation Parameters for EcGFP and H9

molecule	λ_x nm)	pH	k_{0i} (kHz)	F_i (%)	k_{ip} (kHz)	k_{id} (kHz)
EcGFP	405	7.4	0.9 ± 0.9	9 ± 2	0.1 ± 0.1	0.8 ± 0.8
	405	5.5	6.1 ± 0.7	80 ± 10	5.0 ± 0.8	1.1 ± 0.8
	488	7.4	0.3 ± 0.9	10 ± 1	0.1 ± 0.1	0.3 ± 0.6
H9	488	9	0.3 ± 0.3	16 ± 2	0.05 ± 0.05	0.3 ± 0.2
	488	5.2	1.5 ± 1.0	27 ± 4	0.9 ± 0.5	0.6 ± 0.4
	405	9	0.5 ± 0.5	90 ± 10	0.5 ± 0.4	0.05 ± 0.05
	405	5.2	10 ± 4	28 ± 2	6 ± 2	3.8 ± 1.5

At low pH (5.5), the internal protonation quantum yields resulting from fitting the flicker dark fractions using the model of EcGFP are $\phi_{BA} \sim 3 \times 10^{-3}$ and $\phi_{AB} \sim 2 \times 10^{-2}$, respectively, which are in reasonable agreement with the experimental values $\phi_i \sim 3 \times 10^{-3}$ and $\phi_x \sim 1 \times 10^{-2}$, respectively, under 405-nm illumination (Table 1). Note that the quantum yield values are stated with only one digit of precision, reflecting uncertainties due to estimation of the absolute excitation rate and the slope of the flicker rate versus excitation rate. The quantum yield ϕ_{AB} is defined as the probability per excitation that an excited molecule of A will relax into the ground state of B. Good agreement between the model $\phi_{AB} \sim 7 \times 10^{-5}$ and $\phi_{BA} \sim 5 \times 10^{-2}$ and experiment ($\phi_i \sim 5 \times 10^{-2}$) was also obtained at high pH (7.4), where ϕ_i was estimated for the internal protonation flicker in EcGFP. The estimated internal protonation quantum yield of H9 (pH 9 and 405-nm excitation) is $\phi_{AB} \sim 5 \times 10^{-3}$, in good agreement with $\phi_i = 5 \pm 3 \times 10^{-3}$ measured, while the intensity-independent fraction ($\sim 10 \pm 2\%$) under the same conditions was best fit by the model using $\phi_{AN} \sim 50 \times 10^{-3}$, which is larger than the measured value ($\phi_x \sim 10 \times 10^{-3}$). The calculated ϕ_{BA}-value (8×10^{-3}) also agrees well with the measured value (8×10^{-3}) for H9 (pH 9) under 488-nm excitation. In conclusion, the model does account fairly well for the experimental results reported in this work, yet it is not unique.

4.6. Implications on Biological Applications of GFPs. Genetically encoded markers offer superior control over a number of labeling parameters, such as localization, attachment to biomolecules of interest, expression levels, and environmental sensitivity (e.g., Ca^{2+}, Cl^-, I^-, NO_3^-, and H^+). Creation of new mutants with specific environmental and fluorescence properties can be executed in parallel using molecular evolution strategies.[13]

The pHluorins have already been exploited in a number of neuroscience and cell biological applications. Dynamics of single granule exocytosis in RBL-2H3 cells have been visualized, including occasional retrieval and reacidification events.[13] Thus, the balance between exocytosis and endocytosis of single secretory granules is accessible by sensitive, low-background optical methods. Theoretical analysis also predicts that EcGFP pHluorin might be well-suited for studying action-potential-driven exocytosis in neurons[25] while providing the basis for accurate calibration of the fraction of vesicle release. This novel

supereclipticc mutant (pHluorin), which adds the F64L and S65T mutations to standard ecliptic (EcGFP), has higher fluorescence brightness[25] presumably because of the enhancement of the anionic chromophore transition[6] that is expected from these mutations. If F64L and S65T do make the fluorescence properties of supereclipticc more like EGFP than wt-GFP, one would expect enhanced fluorescence excited at 488 nm and possibly a lower tendency to photobleach compared to standard ecliptic. However, since EGFP and wt-GFP both show light-dependent fluorescence photoconversion, it is unlikely that adding F64L and S65T to supereclipticc would eliminate the light dependence of the molecule. EGFP also shows strong pH-dependent flicker from reversible protonation of the chromophore by external protons,[3] which would therefore be expected in supereclipticc as well. An experimental photophysics study of supereclipticc would certainly be helpful toward testing these predictions.

One key advantage of pHluorins over other fluorescence labeling techniques is that only small protons, rather than much larger organic fluorophores, need to move through a membrane pore or fusion pore and into the pHluorin β-barrel to report on vesicular opening events. The role of calcium in the exocytosis rate has been revealed by alkaline-trapping experiments in neurons expressing EcGFP pHluorin,[26] which were previously obscure to FM1-43 experiments.[26] However, despite fast mobility of protons in solution, the response time of GFPs may be an important factor in limiting the minimum response time of an EcGFP probe. The external protonation rate constants $k_+ = 1.93 \pm 0.16 \times 10^{10}$ s^{-1} M^{-1} and deprotonation rate $k_- = 1.1 \pm 0.4 \times 10^3$ s^{-1}, yield a protonation rate of 1.93×10^3 s^{-1} at pH 7 (i.e., a response time of ~0.5 ms). This rate may limit some applications of these probes. Other mutants such as EGFP ($k_- \sim 4.5 \times 10^3$ s^{-1})[3] and citrine ($k_- \sim 9 \times 10^3$ s^{-1})[8] offer faster response but have lower pK_a values.

Care must be taken during the use of GFPs as intracellular pH indicators because of their complex excitation intensity and wavelength-dependent photophysics. Therefore, measurements must be made under constant illumination intensity for quantitative intracellular pH analysis. Furthermore, the time scale (~1 ms) for intrinsic pH-dependent fluorescence fluctuations of these systems might undermine their use for fast time fusion pore fluctuations in individual secretory granules. The pK_a of EcGFP is within the physiological pH range and is therefore advantageous for intracellular molecular pH sensing, compared with other GFPs[25] under many circumstances. The relative invariance of the neutral state fluorescence with pH is also advantageous for cellular visualization under short wavelength illumination. On the other hand, DsRed is highly pH insensitive ($4.4 < \text{pH} < 9$), which provides an alternative with red-shifted fluorescence emission that better avoids cellular autofluorescence.[8]

Recently, comparative studies of the intrinsically fluorescent proteins in live cells and aqueous solution were reported.[57] The main conclusion is that the fluorescence spectra and excited-state lifetimes (i.e., fluorescence quantum yield) of EGFP and DsRed were highly similar in RBL cell cytoplasm, when anchored to the inner leaflet of plasma membrane and in solution. [57] Such similarity suggests that the results of these solution studies will be highly relevant to in vivo biological applications.

Acknowledgment. We kindly thank D. De Angeles and J. Rothman (Memorial Sloan-Kettering Cancer) for samples of pHluorin proteins and R. Y. Tsien (University of California at San Diego) for H9 protein. Research at Cornell was carried out in the Developmental Resource for Biophysical Imaging Optoelectronics with funding provided by the NIH (P41 EB001976) Biomedical Resource and NSF (BIR 8800278). S.T.H. benefited from NSF Graduate Research Fellowship and NIH Molecular Biophysics Training Grant (5 T32 GM08267).

Appendix

Interstate Conversion Kinetics in GFPs. Here we outline the analytical description of the interconversion model, shown schematically in Figure 6, to account for both the light-driven and pH-dependent GFPs fluorescence flicker observed by FCS. In addition, the steady-state spectroscopy (Figure 1) and excited-state dynamics (Figure 2) support three distinct ground states. First, the anionic state (A) of the chromophore is considered as a "bright" state with a large fluorescence quantum yield (0.6−0.7), while the intrinsically neutral (B) state is a relatively dark state with much lower fluorescence quantum yield. The third state in this model is an externally protonated state (N), which is heuristically named quasi-neutral state, and is generated via a reversible binding of an external proton to the anionic chromophore. In our analysis, the $S_0 \rightarrow S_1$ state transitions are treated as instantaneous because of the fact that the excited-state lifetime ($\leq$3.1 ns) is much shorter than the fastest FCS temporal resolution (~200 ns). For simplicity, the triplet state transitions are ignored because the intensities presented are below fluorescence saturation.

For light-driven flicker, an internal protonation reaction (presumably proton displacement between the protein hydrogen-bonding network and the embodied chromophore) occurs between the intrinsically neutral (B) and anionic (A) states,[3] where

$$\mathrm{A} \underset{h\nu_2;k_{BA}}{\overset{h\nu_1;k_{AB}}{\rightleftharpoons}} \mathrm{B} \tag{A1}$$

where the photoconversion rate constants are expected to depend on the excitation photon energy (e.g., $h\nu_1$ and $h\nu_2$). The forward reaction rate constant (k_{AB}) is defined in terms of a quantum yield ϕ_{AB} as follows:

$$k_{AB} = (-\mathrm{d}[A]/\mathrm{d}t)/[A] = \phi_{AB}k_x^{(A)} + k_{ip} \tag{A2}$$

where $k_x^{(A)}$ is the excitation rate for species A, t is time, and k_{ip} is the conversion rate in the dark (when $k_x^{(A)} = 0$), which has a nonzero value at low pH under 405-nm excitation. Considering the reverse conversion rate (k_{BA}) between the two states, the sum of forward and reverse reaction rates can be written as

$$k_{sum}^{AB} = k_{AB} + k_{BA} = \phi_{AB}k_x^{(A)} + \phi_{BA}k_x^{(B)} + k_{ip} + k_{id} \tag{A3}$$

where the internal protonation (k_{ip}) and deprotonation (k_{id}) are the spontaneous forward and reverse reaction rates in the absence of light, which can be determined by extrapolation as $k_x \rightarrow 0$. These rates tend to be small for the anionic state transition at high pH (Table 2).

For pH-dependent flicker, an external protonation reaction occurs between both A and N states,[3] where

$$\mathrm{A} + \mathrm{H}^+ \underset{k_+}{\overset{k_-}{\rightleftharpoons}} \mathrm{N} \tag{A4}$$

where $k_0^{NA} = k_-$, $k_0^{AN} = k_+[H^+]$, and the sum (k_P) of both forward (k_+) and backward (k_-) rates of the pH-dependent conversion can be written as

$$k_P = k_+[H^+] + k_- \tag{A5}$$

with the assumption that $[N] \ll [H^+]$. On the other hand, the flicker fraction (i.e., the average molecular population that resides in the dark state at any given time) can be written as

$$f_{dark} = [\text{molecules in the dark state}]/[\text{molecules in the bright and dark state(s)}] \quad \text{(A6)}$$

where brackets indicate concentrations of the bright and dark states. The values for k_+ and k_- can be determined from the measured FCS flicker rate as a function of pH.

The temporal evolution of the ground B-, N-, and A-state populations, in the schematic model depicted in Figure 6, is described by the following differential equations:

$$\frac{d}{dt}[B] = -k_x^{(B)}\phi_{BA}[B] + k_x^{(A)}\phi_{AB}[A] - k_{id}[B] + k_{ip}[A] \quad \text{(A7)}$$

$$\frac{d}{dt}[A] = -k_x^{(A)}\phi_{AB}[A] + k_x^{(B)}\phi_{BA}[B] + k_{id}[B] - k_{ip}[A] - k_+[A][H^+] + k_-[N] \quad \text{(A8)}$$

$$\frac{d}{dt}[N] = -k_x^{(N)}\phi_{NA}[N] + k_x^{(A)}\phi_{AN}[A] + k_+[H^+][A] - k_-[N] \quad \text{(A9)}$$

where [B], [A], and [N] are the molecular populations of B, A, and N species, which can be excited at rates $k_x^{(A)}$, $k_x^{(B)}$, and $k_x^{(N)}$, respectively. Quantum yields for photoconversion ϕ_{XY} denote initial state X and final state Y (e.g., ϕ_{AB} is from A to B). Direct transitions between N and B are not allowed because the internal protonation site is presumed to not exchange protons directly with the buffer (see above), although B to N can occur via A. Solving eqs A7−A9 under steady-state conditions (i.e., $d/dt\,[A] = d/dt\,[B] = d/dt\,[N] = 0$) yields an estimate for the corresponding population fraction f_{ij}, which corresponds to the measured dark population fractions due to flicker between i and j states:

$$f_{AB} = \frac{[B]}{[A]+[B]+[N]} \quad \text{(A10)}$$

$$= \left[1 + \frac{k_x^{(B)}\phi_{BA} + k_{id}}{k_x^{(A)}\phi_{AB} + k_{ip}} + \left[\frac{k_+[H^+] + k_x^{(A)}\phi_{AN}}{k_- + k_x^{(N)}\phi_{NA}}\right] / \left[\frac{k_x^{(A)}\phi_{AB} + k_{ip}}{k_x^{(B)}\phi_{BA} + k_{id}}\right]\right]^{-1}$$

$$f_{BN} = \frac{[N]}{[A]+[B]+[N]} \quad \text{(A11)}$$

$$= \left\{1 + \frac{k_- + k_x^{(N)}\phi_{NA}}{k_+[H^+] + k_x^{(A)}\phi_{AN}} + \left[\frac{k_x^{(A)}\phi_{AB} + k_{ip}}{k_x^{(B)}\phi_{BA} + k_{id}}\right] / \left[\frac{k_+[H^+] + k_x^{(A)}\phi_{AN}}{k_- + k_x^{(N)}\phi_{NA}}\right]\right\}^{-1}$$

$$f_{AN} = \frac{[N]}{[A]+[N]} = \left[1 + \frac{k_- + k_x^{(N)}\phi_{NA}}{k_+[H^+] + k_x^{(A)}\phi_{AN}}\right]^{-1} \quad \text{(A12)}$$

where the slight difference in functional form for f_{AN} results from the fast time scale for flicker between A and N compared with between A and B. Now, we consider a few special cases that are experimentally relevant.

Dark Fraction in the Limit of Zero Excitation. In the absence of light, the dark fraction for external protonation flicker between A and N is given by

$$f_{AN} = \frac{[N]}{[A]+[N]} = \frac{k_+[H^+]}{k_+[H^+] + k_-} \quad \text{(A13)}$$

and for internal protonation flicker in the absence of light

$$f_{AB} = \left[1 + \frac{k_{id}}{k_{ip}} + \frac{k_+[H^+]k_{id}}{k_-k_{ip}}\right]^{-1} \quad \text{(A14)}$$

Evaluating eqs A13 and A14 using rate constants for EGFP as an example, $k_+ = 1.53 \times 10^9\ M^{-1}\ s^{-1}$, $k_- = 4.5 \times 10^3\ s^{-1}$, and $k_{id}/k_{ip} = 7.55$,[3] we obtain $f_{AN} = 0.77$ at pH 5, and at pH ~10, we find $f_{AB} = 0.12$, in good agreement with the measured values of ~0.80 and 0.13, reported at pH 5 and ~8−11, respectively.[3]

Dark Fraction in the Limit of Bright Excitation. In the limit of high excitation rate (yet well below fluorescence saturation), the expressions for the dark fractions can be simplified to

$$f_{AB} \rightarrow \left[1 + \frac{k_x^{(B)}\phi_{BA}}{k_x^{(A)}\phi_{AB}} + \left[\frac{k_x^{(A)}\phi_{AN}}{k_x^{(N)}\phi_{NA}}\right] / \left[\frac{k_x^{(A)}\phi_{AB}}{k_x^{(B)}\phi_{BA}}\right]\right]^{-1} \quad \text{(A15)}$$

$$f_{AN} \rightarrow \left[1 + \frac{k_x^{(N)}\phi_{NA}}{k_x^{(A)}\phi_{AN}}\right]^{-1} \quad \text{(A16)}$$

$$f_{BN} \rightarrow \left\{1 + \frac{k_x^{(N)}\phi_{NA}}{k_x^{(A)}\phi_{AN}} + \left[\frac{k_x^{(A)}\phi_{AB}}{k_x^{(B)}\phi_{BA}}\right] / \left[\frac{k_x^{(A)}\phi_{AN}}{k_x^{(N)}\phi_{NA}}\right]\right\}^{-1} \quad \text{(A17)}$$

If the excitation rates $k_x^{(A)}$, $k_x^{(B)}$, and $k_x^{(N)}$ are linearly related to each other for a given molecule and excitation wavelength, and the quantum yields for flicker are independent of intensity, then the flicker fractions will approach constant values given by eqs A15−A17, at intensities where the light-driven kinetics are much faster than the spontaneous ground-state kinetics. This prediction explains the constant flicker fraction in T203F and T203Y where the flicker rate is strongly intensity dependent and the zero-intensity rate extrapolation (rate of spontaneous kinetics) is zero.[5]

List of Symbols and Abbreviations

RaGFP = Ratiometric GFP
EcGFP = Ecliptic GFP
H9 = Sapphire GFP (mutations S202F and T203I)
wt-GFP = Wild-type GFP
EGFP = Enhanced GFP (mutations F64L and S65T)

Experimental Symbols

$G(\tau)$ = Autocorrelation
τ = Time Delay
ω = Ratio of Axial (z_0) to Lateral (r_0) Dimensions
N = Number of molecules
f_i = Molecular Dark Fraction (FCS)
λ_x = Excitation Wavelength
I = Excitation Intensity
$k_x^{(A)}$ = Excitation Rate, Species A
σ = Excitation Cross Section
ϵ = Molar Extinction Coefficient
τ_D = Diffusion Time (FCS)

τ_i = Flicker Characteristic Time (FCS) or Fluorescence Decay Time (TCSPC)
$\langle\tau_{fl}\rangle$ = Average Fluorescence Lifetime
a_i = Amplitude Fraction (TCSPC)
ϕ_i = pH-independent Flicker Quantum Yield (FCS)
ϕ_x = pH-dependent Flicker Quantum Yield (FCS)
k_i = pH-independent Flicker Rate (FCS)
k_{0i} = Zero Excitation Intensity Extrapolation of pH-independent Flicker Rate (FCS)
k_P = pH-dependent Flicker Rate (FCS)
F_i = Dark Fraction for pH-independent Flicker
Φ_{fl} = Fluorescence Quantum Yield
Φ_b = Photobleaching Quantum Yield

Symbols Used in the Model

A = Anionic State
B = Internally Protonated Quasi-Neutral State
N = Externally Protonated Neutral State
[X] = Concentration of Species X
ϕ_{AB} = Quantum Yield for Photoconversion from State A to B (Model)
k_{ip} = Internal Protonation Rate Constant (A to B)
k_{dp} = Internal Deprotonation Rate Constant (B to A)
k_+ = External Protonation Rate Constant (A to N)
k_- = External Deprotonation Rate Constant (N to A)

References and Notes

(1) Chalfie, M.; Kain, S. *Green Fluorescent Protein: Properties, Applications, and Protocols*; Wiley-Liss: New York, 1998.
(2) Tsien, R. Y. *Annu. Reυ. Biochem*. **1998**, *67*, 509.
(3) Haupts, U.; Maiti, S.; Schwille, P.; Webb, W. W. *Proc. Natl. Acad. Sci. U.S.A.* **1998**, *95*, 13573.
(4) van Thor, J. J.; Gensch, T.; Hellingwerf, K. J.; Johnson, L. N. *Nat. Struct. Biol.* **2002**, *9*, 37.
(5) Schwille, P.; Kummer, S.; Heikal, A. A.; Moerner, W. E.; Webb, W. W. *Proc. Natl. Acad. Sci. U.S.A.* **2000**, *97*, 151.
(6) Heikal, A. A.; Hess, S. T.; Webb, W. W. *Chem. Phys.* **2001**, *274*, 37.
(7) Dickson, R. M.; Cubitt, A. B.; Tsien, R. Y.; Moerner, W. E. *Nature* **1997**, *388*, 355.
(8) Heikal, A. A.; Hess, S. T.; Baird, G. S.; Tsien, R. Y.; Webb, W. W. *Proc. Natl. Acad. Sci. U.S.A.* **2000**, *97*, 11996.
(9) Cotlet, M.; Hofkens, J.; Maus, M.; Gensch, T.; Van der Auweraer, M.; Michiels, J.; Dirix, G.; Van Guyse, M.; Vanderleyden, J.; Visser, A. J. W. G.; De Schryver, F. C. *J. Phys. Chem. B* **2001**, *105*, 4999.
(10) Chattoraj, M.; King, B. A.; Bublitz, G. U.; Boxer, S. G. *Proc. Natl. Acad. Sci. U.S.A.* **1996**, *93*, 8362.
(11) Lossau, H.; Kummer, A.; Heinecke, R.; PollingerDammer, F.; Kompa, C.; Bieser, G.; Jonsson, T.; Silva, C. M.; Yang, M. M.; Youvan, D. C.; MichelBeyerle, M. E. *Chem. Phys.* **1996**, *213*, 1.
(12) Hanson, G. T.; McAnaney, T. B.; Park, E. S.; Rendell, M. E. P.; Yarbrough, D. K.; Chu, S. Y.; Xi, L. X.; Boxer, S. G.; Montrose, M. H.; Remington, S. J. *Biochemistry* **2002**, *41*, 15477.
(13) Miesenbock, G.; De Angelis, D. A.; Rothman, J. E. *Nature* **1998**, *394*, 192.
(14) Baird, G. S.; Zacharias, D. A.; Tsien, R. Y. *Proc. Natl. Acad. Sci. U.S.A.* **2000**, *97*, 11984.
(15) Miyawaki, A.; Griesbeck, O.; Heim, R.; Tsien, R. Y. *Proc. Natl. Acad. Sci. U.S.A.* **1999**, *96*, 2135.
(16) Kuner, T.; Augustine, G. J. *Neuron* **2000**, *27*, 447.
(17) Galietta, L. J. V.; Haggie, P. M.; Verkman, A. S. *FEBS Lett.* **2001**, *499*, 220.
(18) Kneen, M.; Farinas, J.; Li, Y. X.; Verkman, A. S. *Biophys. J.* **1998**, *74*, 1591.
(19) Guerrero, G.; Siegel, M. S.; Roska, B.; Loots, E.; Isacoff, E. Y. *Biophys. J.* **2002**, *83*, 3607.
(20) Siegel, M. S.; Isacoff, E. Y. *Neuron* **1997**, *19*, 735.
(21) Suhling, K.; Siegel, J.; Phillips, D.; French, P. M. W.; Leveque-Fort, S.; Webb, S. E. D.; Davis, D. M. *Biophys. J.* **2002**, *83*, 3589.
(22) Li, Z. Y.; Murthy, V. N. *Neuron* **2001**, *31*, 593.
(23) Wouters, F. S.; Verveer, P. J.; Bastiaens, P. I. H. *Trends Cell Biol.* **2001**, *11*, 203.
(24) Umeda, T.; Okabe, S. *Neurosci. Res.* **2001**, *40*, 291.
(25) Sankaranarayanan, S.; De Angelis, D.; Rothman, J. E.; Ryan, T. A. *Biophys. J.* **2000**, *79*, 2199.
(26) Sankaranarayanan, S.; Ryan, T. A. *Nat. Neurosci.* **2001**, *4*, 129.
(27) Schoonderwoert, V. T. G.; Martens, G. J. M. *J. Membr. Biol.* **2001**, *182*, 159.
(28) Hess, S. T.; Huang, S.; Heikal, A. A.; Webb, W. W. *Biochemistry* **2002**, *41*, 697.
(29) Widengren, J.; Mets, U.; Rigler, R. *J. Phys. Chem* **1995**, *99*, 13368.
(30) Hess, S. T.; Webb, W. W. *Biophys. J.* **2002**, *83*, 2300.
(31) Lakowicz, J. R. *Principles of Fluorescence Spectroscopy*; Plenum Press: New York, 1983.
(32) O'Connor, D. V.; Phillips, D. *Time-Correlated Single-Photon Counting*; Academic Press: London; Orlando, 1984.
(33) Heim, R.; Prasher, D. C.; Tsien, R. Y. *Proc. Natl. Acad. Sci. U.S.A.* **1994**, *91*, 12501.
(34) Brown, E. B.; Wu, E. S.; Zipfel, W.; Webb, W. W. *Biophys. J.* **1999**, *77*, 2837.
(35) Swaminathan, R.; Hoang, C. P.; Verkman, A. S. *Biophys. J.* **1997**, *72*, 1900.
(36) Terry, B. R.; Matthews, E. K.; Haseloff, J. *Biochem. Biophys. Res. Commun.* **1995**, *217*, 21.
(37) Miyawaki, A.; Tsien, R. Y. *Methods Enzymol.* **2000**, *327*, 472.
(38) Kummer, A. D.; Kompa, C.; Lossau, H.; Pollinger-Dammer, F.; Michel-Beyerle, M. E.; Silva, C. M.; Bylina, E. J.; Coleman, W. J.; Yang, M. M.; Youvan, D. C. *Chem. Phys.* **1998**, *237*, 183.
(39) Kummer, A. D.; Wiehler, J.; Rehaber, H.; Kompa, C.; Steipe, B.; Michel-Beyerle, M. E. *J. Phys. Chem. B* **2000**, *104*, 4791.
(40) McAnaney, T. B.; Park, E. S.; Hanson, G. T.; Remington, S. J.; Boxer, S. G. *Biochemistry* **2002**, *41*, 15489.
(41) Ward, W. W.; Cormier, M. J. *J. Biol. Chem.* **1979**, *254*, 781.
(42) Miyawaki, A. *Cell Struct. Funct.* **2002**, *27*, 343.
(43) Voityuk, A. A.; Michel-Beyerle, M. E.; Rosch, N. *Chem. Phys. Lett.* **1998**, *296*, 269.
(44) Weber, W.; Helms, V.; McCammon, J. A.; Langhoff, P. W. *Proc. Natl. Acad. Sci. U.S.A.* **1999**, *96*, 6177.
(45) Mizuno, H.; Sawano, A.; Eli, P.; Hama, H.; Miyawaki, A. *Biochemistry* **2001**, *40*, 2502.
(46) Patterson, G. H.; Lippincott-Schwartz, J. *Science* **2002**, *297*, 1873.
(47) Elsliger, M. A.; Wachter, R. M.; Hanson, G. T.; Kallio, K.; Remington, S. J. *Biochemistry* **1999**, *38*, 5296.
(48) Brejc, K.; Sixma, T. K.; Kitts, P. A.; Kain, S. R.; Tsien, R. Y.; Ormo, M.; Remington, S. J. *Proc. Natl. Acad. Sci. U.S.A.* **1997**, *94*, 2306.
(49) Voityuk, A. A.; MichelBeyerle, M. E.; Rosch, N. *Chem. Phys. Lett.* **1997**, *272*, 162.
(50) Voityuk, A. A.; Michel-Beyerle, M. E.; Rosch, N. *Chem. Phys.* **1998**, *231*, 13.
(51) Voityuk, A. A.; Kummer, A. D.; Michel-Beyerle, M. E.; Rosch, N. *Chem. Phys.* **2001**, *269*, 83.
(52) Ormo, M.; Cubitt, A. B.; Kallio, K.; Gross, L. A.; Tsien, R. Y.; Remington, S. J. *Science* **1996**, *273*, 1392.
(53) Creemers, T. M. H.; Lock, A. J.; Subramaniam, V.; Jovin, T. M.; Volker, S. *Proc. Natl. Acad. Sci. U.S.A.* **2000**, *97*, 2974.
(54) van Thor, J. J.; Pierik, A. J.; Nugteren-Roodzant, I.; Xie, A. H.; Hellingwerf, K. J. *Biochemistry* **1998**, *37*, 16915.
(55) Jung, G.; Mais, S.; Zumbusch, A.; Brauchle, C. *J. Phys. Chem. A* **2000**, *104*, 873.
(56) Ward, W. W. Biochemical and Physical Properties of Green Fluorescent Protein. In *Green Fluorescent Protein: Properties, Applications, and Protocols*; Chalfie, M., Kain, S., Eds.; Wiley-Liss: New York, 1998; p 45.
(57) Hess, S. T.; Sheets, E. D.; Wagenknecht-Wiesner, A.; Heikal, A. A. *Biophys. J.* **2003**, *85*, 2566.